The Planck-LFI instrument: Analysis of the $1/f$ noise and implications for the scanning strategy

D. Maino[1], C. Burigana[2], M. Maltoni[2,3,4], B.D. Wandelt[5], K.M. Górski[5,6,7], M. Malaspina[2], M. Bersanelli[8], N. Mandolesi[2], A.J. Banday[9], and E. Hivon[10]

[1] SISSA, International School for Advanced Studies, Via Beirut 2-4, I-34014 Trieste, Italy
[2] Istituto TeSRE, Consiglio Nazionale delle Ricerche, Via Gobetti 101, I-40129 Bologna, Italy
[3] Dipartimento di Fisica, Universitá di Ferrara, Via Paradiso 12, I-44100 Ferrara, Italy
[4] INFN, Sezione di Ferrara, Via Paradiso 12, I-44100 Ferrara, Italy
[5] TAC, Theoretical Astrophysics Center, Juliane Maries Vej 30, DK-2100 Copenhagen, Denmark
[6] ESO, European Southern Observatory, Karl-Schwarzschild Str. 2, D-85748, Garching, Germany
[7] Warsaw University Observatory, Warsaw, Poland
[8] IFC, Consiglio Nazionale delle Ricerche, Via Bassini 15, I-20133 Milano, Italy
[9] MPA, Max Planck Inst. für Astrophysik, Karl-Schwarzschild Str. 1, D-85740, Garching, Germany
[10] CalTech, California Institute of Technology, 1200 East California Boulevard, CA-91125, Pasadena, U.S.A.

Abstract. We study the impact of $1/f$ noise on the PLANCK Low Frequency Instrument (LFI) observations (Mandolesi et al. 1998) and describe a simple method for removing striping effects from the maps for a number of different scanning strategies. A configuration with an angle between telescope optical axis and spin-axis just less than $90°$ (namely $\simeq 85°$) shows good destriping efficiency for all receivers in the focal plane, with residual noise degradation $< 1-2\%$. In this configuration, the full sky coverage can be achieved for each channel separately with a $5°$ spin-axis precession to maintain a constant solar aspect angle.

Key words: methods: data analysis — cosmology: cosmic microwave background — space vehicles

1. Introduction

Since the great success of *COBE*-DMR results (Smoot et al. 1992; Bennet et al. 1996a; Górski et al. 1996) and a large number of ground-based and balloon-borne detections of cosmic microwave background (CMB) anisotropy, many experiments with sensitivities and angular resolutions better than *COBE* are expected for the near future [e.g. Lasenby et al. (1998) and De Bernardis & Masi (1998) for a review].

Send offprint requests to: maino@sissa.it

It is also clear that only a space mission free from unwanted contamination from ground and Earth atmosphere and with a nearly full-sky coverage (Danese et al. 1996) can fully exploit the gold mine of cosmological and astrophysical (De Zotti et al. 1999) information imprinted in the small scale pattern of microwave sky anisotropy. The two space missions MAP (Microwave Anisotropy Probe) (see Bennet et al. 1996b) by NASA and PLANCK (Mandolesi et al. 1998; Puget et al. 1998) by ESA, planned to be launched respectively in the year 2001 and 2007, will play a definitive role to fully understand the properties and the evolution of the universe.

As for any CMB experiment, great attention has to be devoted to all the possible systematic effects. In the context of the PLANCK mission we have carried out a detailed study of one of these effects: the so-called $1/f$, or low-frequency, noise which may lead to unwanted stripes in the final sky maps. Such stripes can increase the overall noise level and introduce correlations which affect adversely the statistical analysis of the CMB anisotropy. Recent analytical work by Seiffert et al. (1997) has shown the dependency of the $1/f$ noise upon the radiometer characteristics such as the bandwidth, the noise temperature, payload environment temperature and other quantities properly related to PLANCK-LFI radiometers. They can be combined to define a representative parameter, the "knee-frequency" f_k, which has to be kept as low as possible compared with the spinning frequency f_s of the spacecraft. Janssen et al. (1996) have indeed demonstrated that for $f_k \gtrsim f_s$ a degradation in final sensitivity will result.

In Sect. 2 we briefly outline the source of the $1/f$ noise and its spectral shape. In Sect. 3 we report the framework of our simulations, evaluate the possible impact of $1/f$ noise and present the technique for removing the $1/f$ noise in the context of PLANCK-LFI. The main results both for un-reduced and reduced $1/f$ noise are presented in Sect. 4. Our main conclusions and implications for the scanning strategy are discussed in Sect. 5.

2. Source of $1/f$ noise

The $1/f$ noise of the PLANCK-LFI receivers is generated by High Electron Mobility Transistor (HEMT) amplifier gain instabilities. If not properly corrected, it may lead to stripes in the final maps due to the satellite scanning strategy. Therefore it is of great importance to reduce the impact of such effect both by hardware and software techniques. The LFI receiver concept is driven by the need to reduce instability effects. Bersanelli et al. (1995) described the design of LFI radiometers which are modified Blum correlation receivers (Blum 1959; Colvin 1961). We remind the interested reader to the Bersanelli et al. (1995) and Seiffert et al. (1997) works for an analytical analysis of the source of $1/f$ noise in the final output of this receiver design and of the dependency of f_k upon the radiometer properties. In general the noise power spectrum writes:

$$S_{\mathrm{noise}}(f) = a \left[1 + \left(\frac{f_k}{f} \right)^{\beta} \right] , \qquad (1)$$

where a is a normalization factor (related to the ideal white noise level of the receiver) and β takes typical theoretical values from 1 to 2.5 depending on the source of noise (gain drifts or thermal effects): $\beta = 1$ is the $1/f$ noise case. It is also a good approximation to take $S_{\mathrm{noise}}(f)$ vanishing for $f < f_{\min}$ and for $f > f_{\max}$. Delabrouille (1998) proposed $f_{\min} \sim 1/T_{\mathrm{mission}}$ and $f_{\max} \sim 1/2T_{\mathrm{sampling}}$.

With the current instrument specifications (Mandolesi et al. 1998) typical values of the knee-frequency are $f_k = 0.046$ Hz and $f_k = 0.11$ Hz at 30 and 100 GHz repsectively with a 20 K load. Lower values of f_k can be reached by lowering the load temperature possibly up to values ($\simeq 4$ K) close to the full (sky plus environment) signal entering the horn (Seiffert et al. 1997).

3. Scan circles, sky maps and destriping

As reported in Mandolesi et al. (1998), the selected orbit for PLANCK satellite will be a Lissajous orbit around the L2 Lagrangian point of the Sun-Earth system. The spacecraft spins at 1 rpm and the spin axis is kept on the Ecliptic plane at constant solar angle by repointing of $2.5'$ every hour. The field of view of the two instruments is between $\alpha \approx 80° - 90°$ from the spin-axis direction. Hence

PLANCK will trace large circles in the sky: these circles cross each other in regions close to the Ecliptic poles. The shape and width of these regions depend upon the angle α, the scanning strategy and beam location in the focal plane. The value of the angle α has not yet been fully defined, as well as the scanning strategy, which may or may not include a periodic motion of the spin-axis away from the Ecliptic plane. These options depend on a trade-off between different systematic effects (striping, thermal effects, straylight), which have to be carefully addressed.

3.1. The "flight-simulator"

Burigana et al. (1997, 1998) have described in detail the code we have implemented for the PLANCK scanning strategy and we refer the reader to these papers. The relevant geometrical inputs are the beam location in the focal plane and the angle α between the spin and pointing axis.

For each beam position on the focal plane our code outputs the complete data stream. We consider here a reduced version of the actual baseline for the scanning strategy (actual parameters in parentheses): spin-axis shift of $5'$ every 2 hours (instead of $2.5'$ every hour) and three samplings per FWHM of $30'$ at 30 GHz (instead of 12 samplings every $30'$, i.e. 4 samplings every $10'$, the FWHM at 100 GHz; see Mandolesi et al. 1998). These modifications allow us to explore a large region of the parameter space, beam position, f_k, scanning strategy and pointing angle α, in reasonable time. Furthermore we do not consider the single minute data stream but we take the average over the 120 circles forming a given 2-hours set. In what follows we run simulations for the 30 GHz channel.

Wright (1996) has shown that possible data filtering on a given scan circle may help in reducing the impact of $1/f$ noise. This is useful for values of knee frequency f_k typical for "total power" receivers which are much higher that those considered here and therefore we chose not to include this technique here.

In general both the white noise sensitivity and the knee-frequency depend on the actual temperature in the sky T_x seen by the horn. Our synthetic model for microwave sky emission includes a standard CDM prediction for CMB fluctuations plus a model of galactic emission. This model has the spatial template from the dust emission (Schlegel et al. 1998) but has been normalized to include contribution from synchrotron, free-free and dust according to *COBE*-DMR results (Kogut et al. 1996). The major foreground contamination at 30 GHz comes from synchrotron and free-free. We then choose to overestimate the overall synchrotron fluctuations by a factor of ≈ 10, leading to a maximum Galaxy emission of $\simeq 44$ mK. This is the worst case scenario with respect to destriping efficiency (see Sects. 3.3 and 3.4).

Of course the impact on the receiver sensitivity of the sky temperature T_x, dominated by the CMB monopole,

T_0, is not critical even including in T_x a typical environment temperature of about 1 K and the pessimistic Galaxy model adopted here, being in any case T_x a small fraction of the noise temperature $T_n \sim 10$ K.

We convolve input maps with a pure symmetric gaussian beam with the nominal FWHM (33′) of the 30 GHz PLANCK-LFI channel: therefore main-beam distortions and stray-light contamination are not considered here.

3.2. Generation of instrumental noise

We have the possibility to generate different kinds of noise spectra. We work in Fourier space and generate the real and imaginary part of Fourier coefficients of our noise signal. After generating a realisation of the real and imaginary part of the Fourier coefficients with spectrum defined in Eq. (1), we FFT (Fast Fourier Transform; Cooley & Tukey 1997; Heideman et al. 1984) them and obtain a real noise stream which has to be normalized to the white noise level. We use the theoretical value of $f_k = 0.05$ Hz at 30 GHz assuming a 20 K load temperature (see Sect. 2). We chose to generate one year of a mission by combination of 16 hour long noise stream ($\sim 2 \ 10^6$ data points) which correspond to 8 spin axis positions: this seems a reasonable compromise among our present knowledge of real hardware behaviour and the required computational time with respect noise stream length. The actual time for a generation of a noise stream 16 hours long and one year of mission even in our reduced scanning strategy is ~ 10 hours on a Silicon Graphics machine with 2 Gb of RAM and clock speed of 225 MHz. We also verified that the most time consuming operation in our code is just the FFT $1/f$ noise generation. Better performances (Wandelt et al. 1999; Wandelt & Górski 1999) may be obtained using noise generation technique in real space (e.g. Beccaria et al. 1996 and Cuoco & Curci 1997 and references therein).

3.3. From data stream to sky maps

The final output of our "flight-simulator" are 4 matrices with a number of rows equal to the considered spin-axis positions n_s (for one year of mission ~ 4320 in our reduced baseline as in Sect. 3.1) and a number of columns equal to the number of integrations, weakly dependent on α, along one scan circle (here $n_p \sim 2160$). The input and output maps are in HEALPix pixelisation scheme (Górski et al. 1998, http:\\www.tac.dk\~healpix); we use an input map with a resolution of about 3.5′ corresponding to 12 million equal area pixels on the full sky.

For each circle, the code outputs are the pixel number $\mathbf{N}$ at the specified resolutions, the temperature plus total (white plus $1/f$ noise) noise contribution $\mathbf{T}$, the temperature with only white noise $\mathbf{W}$ and the pure signal as observed in absence of instrumental noise $\mathbf{G}$. The $\mathbf{W}$ and $\mathbf{G}$ will be used for studying the degradation of $1/f$ noise with respect to the ideal pure white noise case and the impact of scanning strategy geometry on observed pixel temperatures.

We can arbitrarily choose the temperature output data stream resolution from 3.5′ to higher values (smaller resolution) which set also the output temperature map resolution. Regarding the data stream for the pixel number outputs we can also use higher resolutions, allowing to test the impact of using more or less stringent crossing conditions in the destriping algorithm (see the following section).

From these data streams it is quite simple to obtain observed simulated maps: we make use of $\mathbf{N}$ and $\mathbf{T}$ to coadd the temperatures of those pixels observed several times during the mission. In the same way we build maps with only white noise contribution, without receiver noise, as well as a sensitivity map knowing how many times a single pixel is observed.

In Fig. 1 we show a pure noise (white plus $1/f$) map in Ecliptic coordinates after signal subtraction ($\mathbf{T} - \mathbf{G}$): stripes are clearly present.

3.4. Destriping techniques

We developed a simple technique which is able to eliminate gain drifts due to $1/f$ noise. This is derived from the COBRAS/SAMBA Phase A study proposal (Bersanelli et al. 1996) and from a re-analysis of Delabrouille (1998). As reported by Janssen et al. (1996) the effect of $1/f$ noise can be seen as one or more additive levels, different for each scan circle. We worked with averaged (over 2 hours period) scan circles and hence we nearly removed drifts within each circle: what is left is related to the "mean" $1/f$ noise level for this observation period. In fact averaging scan circles into a single ring corresponds to a low-pass filtering operation. As long as f_k is not far larger than the spin frequency, this ensures that only the very lowest frequency components of the $1/f$ noise survive. Therefore it is a good approximation to model the averaged $1/f$ noise as a single constant offset A_i for each ring for the set of parameters we are using. We want to obtain the baselines for all the circles and re-adjust the signals correspondingly.

In order to estimate the different A_i we have to find common pixels observed by different scan circles and the pixel size in the matrix $\mathbf{N}$ is a key parameter. Increasing the resolution used in $\mathbf{N}$ reduces the number of crossings possibly yielding to lower destriping efficiency, while adopting resolutions lower than the resolution of the input map and of the matrix $\mathbf{T}$ introduces extra noise, related to variations of real sky temperature within the scale corresponding to the lower resolution adopted in $\mathbf{N}$, which may introduce artifacts in the destriping code. The adopted pessimistic galactic emission model, which by construction has gradients larger than those inferred by current
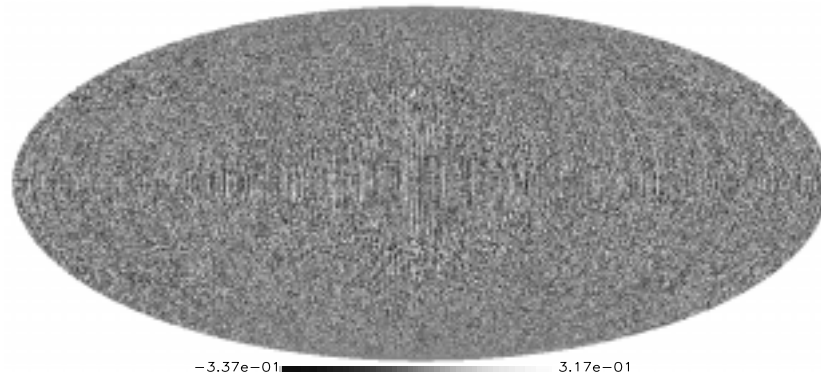
−3.37e−01 ▬   3.17e−01

Fig. 1. Pure noise (white and $1/f$ noise together) map before destriping: stripes are clearly present. The adopted f_k is 0.05 Hz and units are in mK. See the text for simulation input parameters

data, emphasizes this effect and our simulations are then conservative in this respect. In the following N_{il}, T_{il} and E_{il} will denote the pixel number, the temperature and the white noise level for the pixel in the ith row and l^{th} column. Let us denote a generic pair of different observations of the same pixel with an index π which will range between 1 and n_c, the total number of pairs found. In this notation π is related to two elements of $\mathbf{N}$: $\pi \to (il, jm)$ where i and j identify different scan circles and l and m the respective position in each of the two circles.

We want to minimize the quantity:

$$
\begin{aligned}
S &= \sum_{\text{all pairs}} \left[\frac{[(A_i - A_j) - (T_{il} - T_{jm})]^2}{E_{il}^2 + E_{jm}^2} \right] \\
&= \sum_{\pi=1}^{n_c} \left[\frac{[(A_i - A_j) - (T_{il} - T_{jm})]^2}{E_{il}^2 + E_{jm}^2} \right]_\pi
\end{aligned}
\tag{2}
$$

with respect to the unknown levels A_i. The sub-index π indicates that each set of (il, jm) is used in that summation. It is clear that S is quadratic in all the unknown A_i and that only differences between A_i enter into Eq. (2). Therefore the solution is determined up to an arbitrary additive constant (with no physical meaning for anisotropy measurements). We choose then to remove this indetermination by requiring that $\sum_{h=1}^{n_s} A_h = 0$. This is equivalent to replace Eq. (2) with $S' = S + \left(\sum_{h=1}^{n+s} A_h \right)^2$. After some algebra we finally get:

$$
\begin{aligned}
\frac{1}{2} \frac{\partial S'}{\partial A_k} &= \sum_{\pi=1}^{n_c} \left[\frac{[(A_i - A_j) - (T_{il} - T_{jm})] \cdot [\delta_{ik} - \delta_{jk}]}{E_{il}^2 - E_{jm}^2} \right]_\pi \\
&+ \sum_{h=1}^{n_s} A_h = 0
\end{aligned}
\tag{3}
$$

for all the $k = 1, ..., n_s$ (here δ is the usual Kronecker symbol). This translates into a set of n_s linear equation

$$
\sum_{h=1}^{n_s} C_{kh} A_h = B_k, \quad k = 1, ..., n_s
\tag{4}
$$

which can be easily solved. Furthermore we note that by construction the matrix $\mathbf{C}$ of C_{kh} coefficients is symmetric, positive defined and non singular. The first property permits to hold in memory only one half of the matrix $\mathbf{C}$ (e.g. the upper-right part), the second allows us to solve the linear system without having to exchange rows or columns (Strang 1976), so preserving the symmetry. The non-singularity of $\mathbf{C}$ is true provided that there are enough intersections between different circles and hence is related to the resolution at which we look for common pixels between different scan circles, to the scanning strategy and beam location. A detailed discussion of numerical algorithm for solving this system with significant saving of required RAM is presented in Burigana et al. (1997).

It is interesting to note that the applicability of this destriping technique does not depend upon any a-priori assumption about the real value of f_k or the real noise spectral shape since it can work also for different values of the exponent β in Eq. (1).

4. Simulations results and scanning strategy

We first consider an angle $\alpha = 90°$ between telescope and spin axes and a beam location with $(\theta_B, \phi_B) = (2.8°, 45°)$. Here θ_B is the angle from the optical axis: this is a typical value for the 100 GHz (with a $\simeq 1.5$ m aperture off-axis Gregorian telescope) horns while the 30 GHz beams are placed at larger θ_B values. This assumption is therefore conservative with respect to the destriping efficiency, since in this case the region of crossings between scan circles is smaller and closer to Ecliptic poles. The angle ϕ_B is the beam center displacement from the axis given by the intersection between the sky field of view plane and the plane containing the telescope and spin axes (see Burigana et al. 1998). Our choice of $\phi_B = 45°$ is intermediate between 0° (or 180°) and 90° which are equivalent for the destriping
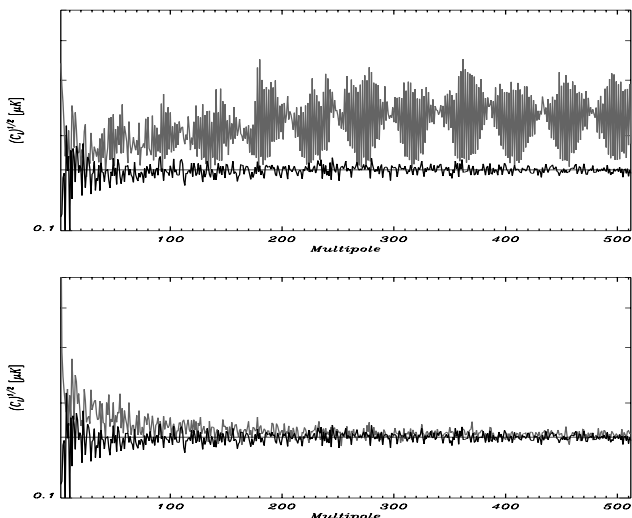
Fig. 2. Top panel: noise power spectra at 30 GHz before destriping. Simulations parameters are: $\alpha = 90°$, $(\theta_B, \phi_B) = (2.8°, 45°)$, $f_k = 0.05$ Hz and spin-axis always on the Ecliptic plane. The white noise spectrum and its theoretical level are also reported for comparison. The excess of noise is about 40% over the white noise level. Bottom panel: noise power spectra after destriping. Now the added noise is only $1 - 2\%$ of the white noise level

respectively to an on-axis beam (with crossings only at Ecliptic poles for $\alpha = 90°$) and a beam which spreads crossings over the wider possible region. The adopted beam location is therefore a non-degenerate case although non optimal.

We evaluated the impact of $1/f$ noise both in terms of added rms noise and of angular power spectrum.

The white noise power spectrum can be derived analytically knowing the total number of pixels in the sky and pixel sensitivity:

$$C_{\ell,wn} = \frac{4\pi}{N_{\mathrm{pix}}^2} \sum_{i=1}^{N_{\mathrm{pix}}} \sigma_i^2 = \frac{4\pi}{N_{\mathrm{pix}}} \langle \sigma^2 \rangle . \qquad (5)$$

4.1. Simulation results

In the top panel of Fig. 2 we show the square root of the power spectrum (which is roughly proportional to rms contribution of temperature per ℓ-bin) before applying the destriping technique: the solid line is the white noise level as derived from Eq. (5) and the superimposed spectrum is derived from a simulation with only white noise included. The agreement is very good which confirms the accuracy of our simulator and map-making algorithm. The gray line is the global noise spectrum (white and $1/f$ noise together). The spectrum is clearly non-white: blobs are present. The excess of noise in terms of both rms and $\sqrt{C_\ell}$ is about 40% of white noise level. Figure 3 shows the recovered baselines and Fig. 4 shows the noise map after

applying our destriping code: stripes are no more evident. This situation can be quantified by computing the noise power spectrum of the destriped map, as shown in the bottom panel of Fig. 2. Now the spectrum is considerably flatter and no more blobs are present, with an overall noise excess of $1 - 2\%$ over the white noise level. This confirms the efficiency of the destriping algorithm, under the above mentioned simplifying assumptions. On the other hand it is clear from the bottom panel of Fig. 2 that at large scales, corresponding to $\ell \lesssim 100$, a non-negligible residual contribution is present in the noise spectrum. A lower knee frequency (achievable with the reference loads at 4 K) is necessary to further reduce the effect.

We also investigated if different scanning strategies may help in destriping efficiency. Possible periodic motion of the spin-axis away from the Ecliptic plane have the effect of broadening the region of crossings between different circles. This goes in the direction of removing possible degeneracies in the destriping system. We implemented both sinusoidal oscillations and precessions: the first does not preserve the spacecraft solar illumination and this is likely to induce thermal effects and drifts in the data.

The second is then preferable, since it keeps the solar angle constant as the satellite moves the spin-axis. For both the motions we performed 10 complete oscillations per year of mission with 10° amplitude. The results before and after destriping are nearly the same for the two cases and Fig. 5 reports noise power spectra for the precession motion: before destriping blobs are still present and disappear after destriping. The excess of noise is $\sim 40\%$ and $1 - 2\%$ before and after destriping respectively.

We consider also a case of an on-axis beam $(\theta_B, \phi_B) = (0°, 0°)$ with $\alpha = 90°$. This situation is representative of horns which, in the focal plane arrangement, are placed close to the scanning direction: from the destriping point of view these horns are indeed equivalent to on-axis horns and intersections between different scan circles are nearly only at Ecliptic poles. This represents a degenerate situation with respect to destriping efficiency. Figure 6 shows noise power spectra for this on-axis case before and after destriping: the geometry of the simulation is changed and the same for blob shape which is not well defined. Here the level of added noise is $\sim 42\%$. After destriping we are left with an excess of noise of the order of 5% of the white noise and the noise spectrum is considerable less flat than before. Such excess noise and a non-flat spectrum around $\ell \sim 100 - 200$ (where the first CMB Doppler peak is expected) after destriping is clearly not acceptable for the feeds aligned with the scan direction. Moving the spin axis is a way to remove this degeneracy, as well as to complete the sky coverage for all channels.

Keeping fixed the beam position we move the angle α from 90° to 85°: this of course leaves small regions around Ecliptic poles which are not observed but has the advantage to enlarge the scan circle crossing region. Figure 7
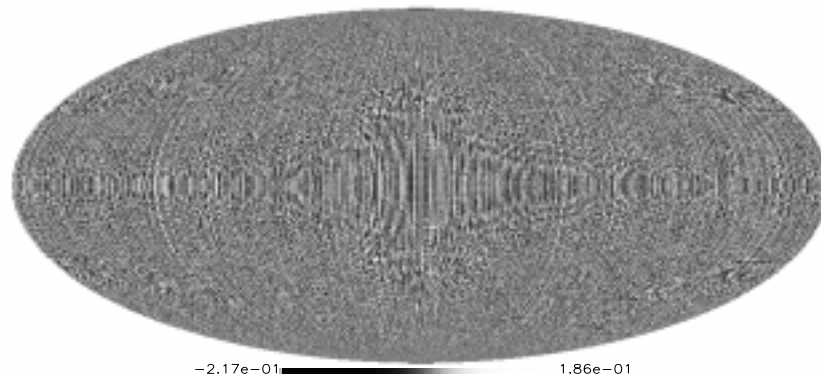
Fig. 3. Baselines recovered from destriping algorithm for the case reported in Fig. 1
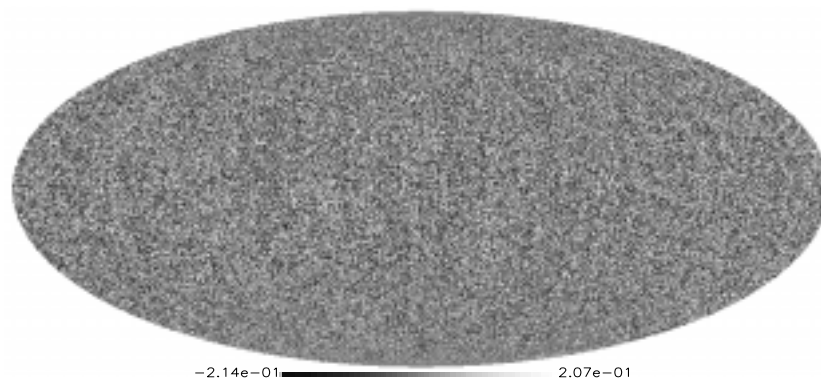

Fig. 4. Noise map after destriping for the same case illustrated in Fig. 1: stripes are no more visible

shows noise power spectra before and after destriping for this 85°, on-axis case: now blobs are clearly visible with dimensions in ℓ-space different from Fig. 2 due to different geometrical configuration. These blobs are completely removed after destriping leaving a level of added noise after destriping of only $\lesssim$ 2% over the white noise. This is essentially what we obtained for the off-axis configuration. All the simulations considered so far were performed with a $f_k = 0.05$ Hz, a "reference" value close to that predicted by Seiffert et al. (1997) for a reference load at 20 K.

To decrease the residual effect, a 4 K reference load is being designed. In this configuration the theoretical knee frequency would be less than 10 mHz. We chose to run a simulation with $f_k = 0.01$ Hz with the usual off-axis configuration with $\alpha = 90°$. As for the other cases we report noise power spectra before and after destriping in Fig. 8. It is interesting to note that now the level of added noise is 9% before destriping and reduces only to 0.5% after applying destriping algorithm.

4.2. Morphology of the C_ℓ artefacts due to $1/f$ noise

We now give a short theoretical argument for the expected morphology of the C_ℓ power spectra of the simulated striping pattern. For scanning without wobbling or precession, two angular scales fully determine the structure of the striping pattern on the sky. One is the half opening angle $\lambda_1 = 90°$ of the ecliptic equator which the spin axis traces on the sky as PLANCK completes a full orbit about the Sun. This makes the noise pattern symmetric under parity, on average. The other scale is the half opening angle of the scanning rings $\lambda_2 \simeq \alpha - \theta_B \sin(\phi_B)$, $\theta_B \ll \pi/2$.

The combination of these two nearby scales leads to beats in the C_ℓ, which are visually apparent as the "blob" in the top panels of Figs. 2, 5, 6, 7, 8. Treating this effect in the same way as the appearance of fringes in an interference pattern we can calculate the width in ℓ of each blob as $\Delta\ell = 90/(\lambda_2 - \lambda_1)$. This is in quantitative agreement with our numerically computed spectra. It also explains the absence of beats in the top panel of Fig. 6, where $\lambda_2 = \lambda_1 = 90°$ and the power spectrum can be understood as a single blob with infinite $\Delta\ell$.
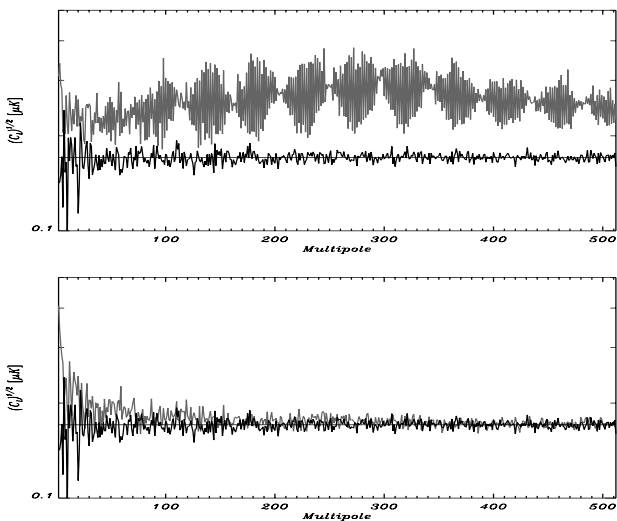
Fig. 5. Top panel: noise power spectra at 30 GHz before destriping. Simulation parameters are the same of Fig. 2 except for the scanning strategy which includes here precession (see the text). The added noise is $\sim 40\%$ of the white noise level. White noise spectra are also reported for comparison. Bottom panel: noise power spectra after destriping. Again, the added noise is now only $1 - 2\%$ of the white noise level
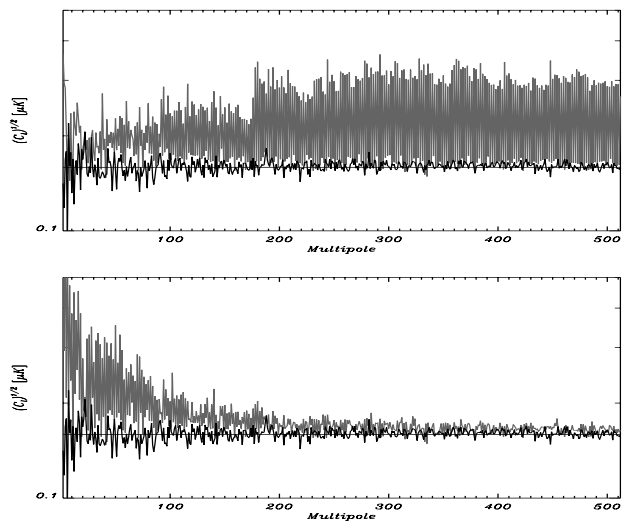
Fig. 6. Top panel: noise power spectra at 30 GHz before destriping. Simulation parameters are the same of Fig. 2 but the beam position is now $(\theta_B, \phi_B) = (0°, 0°)$. The added noise is $\sim 42\%$ of the white noise level. White noise spectra are also reported for comparison. Bottom panel: noise power spectra after destriping. The added noise is now larger than previous cases, being 5% of the white noise level

For scanning strategies with some kind of "wobble" the correlation function will still be approximately symmetric if the amplitude of the wobble is small compared to 90° and the above statements remain approximately true although a weakly symmetry breaking can be seen in the top panel of Fig. 5, where the beats do not reach all the way down to the white noise level.

The offset of the blobs compared to the white noise level is given by the rms excess power due to the $1/f$ noise component.

5. Discussion and conclusion

We have reported here an extensive study of the $1/f$ noise contamination for different scanning strategies, beam location on the focal plane as well as for different values of the knee frequency. Even in this idealised situation (all other systematics are well under control) we can gain useful information from our study.

First of all from these simulations it seems that moving the spin-axis away from the ecliptic plane does not significantly help the destriping efficiency for typical LFI beam locations and, concerning the $1/f$ noise alone as source of drifts, it would be preferable to keep the spin-axis always on the Ecliptic plane. This is clear when we compare results as those in the bottom panels of Fig. 2 and Fig. 5 which are practically identical.

Furthermore for most of the LFI beams the choice of $\alpha = 90°$ would be acceptable: the destriping left only $\lesssim 2\%$ of excess noise with respect to the pure white noise
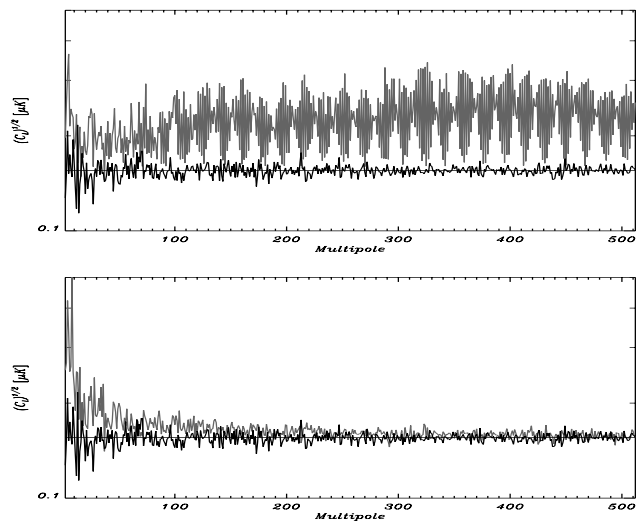
Fig. 7. Top panel: noise power spectra at 30 GHz before destriping. Simulation parameters are the same of Fig. 6 but the angle α is now set to 85°. The added noise is $\sim 42\%$ of the white noise level. White noise spectra are also reported for comparison. Bottom panel: noise power spectra after destriping. The added noise is now only 2% of the white noise level

case. On the other hand, some LFI beams are equivalent to on-axis beam which, from the bottom panel of Fig. 6, is clearly a degenerate case. A smaller value of α (namely 85°) breaks this degeneracy at an acceptable level yielding the usual destriping efficiency. From these two points an indication of a possible choice of the scanning strategy and instrument configuration arises: with $\alpha = 85°$ and precession of the spin-axis (no thermal drifts) with only

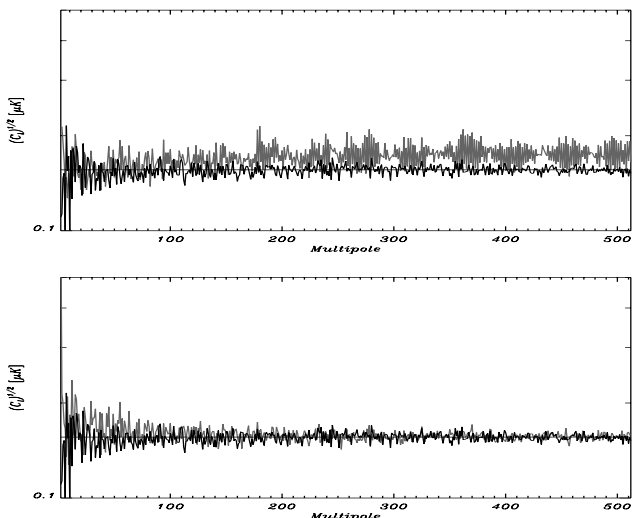**Fig. 8.** Top panel: noise power spectra at 30 GHz before destriping. Simulation parameters are the same of Fig. 2 but now $f_{\mathrm{k}} = 0.01$ Hz. The added noise is now only 9% of the white noise level. White noise spectra are also reported for comparison. Bottom panel: noise power spectra after destriping. The added noise is now only 0.5% larger the white noise level

5° amplitude (half of what we considered here) appears satisfactory for de-striping performances while preserving full-sky coverage for all channels. This allows data redundancy but introduces irregularities in the integration time distribution, which may be an issue for the data analysis. Without spin axis modulations, a quite complete sky coverage and a smooth integration time distribution at each frequency can be achieved only by assembling data from different receivers, losing redundancy.

The whole set of simulations seems to indicate that there is enough redundancy of observations to remove at acceptable level the contamination due to $1/f$ noise even if we require a more strict condition of crossings between scan circles. Of course, the performance of this destriping code could be partially optimized in the future by appropriately choosing the number of levels per circle and the crossing condition according to the dominant kind of instrumental noise (the parameters f_{k} and β), the magnitude of the gradients in the sky emission and our knowledge of other contamination sources. Another point to mention is the possibility of jointly destriping the data from two or more feeds at the same frequency but differently located on the sky field of view: this will enlarge the dimension of the system in Eq. (4) that have to be solved and then RAM requirements. Although feeds in different locations in the focal plane will have different beam shapes and main beam distortions may introduce extra-noise, this is an interesting point particularly with respect "degenerate" feed positions and will be addressed in a future work.

For what concerns properly the $1/f$ noise, an important indication comes from the simulation with $f_{\mathrm{k}} =$

0.01 Hz: the excess of noise before destriping reduces by a factor $\simeq 4 \div 5$ with respect to the case $f_{\mathrm{k}} = 0.05$ Hz, indicating a possible linear relation between the additional rms and knee-frequency. In addition the extra noise level after destriping decreases, at least under these ideal assumptions, by a factor $\simeq 3$. The source of this extra noise after destriping is probably partially due to the $1/f$ noise on time-scales less than the spin-rate. This can be see when comparing the level of extra noise, after destriping, for the $f_{\mathrm{k}} = 0.05$ Hz and $f_{\mathrm{k}} = 0.01$ Hz cases, values larger and smaller than f_{s} respectively.

There are many open issues both astrophysical and instrumental. Regarding the first, the microwave emission model we use, although pessimistic for what concerns galactic emission, can be completed with the inclusion of different foreground contributions. The emission from extragalactic point sources and in particular their variability may decrease our destriping efficiency. We have also not considered here any other source of possible systematic effects such as thermal effects, main beam distortions and stray-light contamination induced by Galaxy emission. These effects may in principle degrade the accuracy in removing $1/f$ noise stripes, by introducing systematic differences in the temperatures observed in the crossing points used in the destriping algorithm: a preliminary analysis of simulations with an elliptical Gaussian beam (instead of the circular symmetry one considered in this work) with a 1.7 ratio between major and minor axis, indicates a small impact of a such effect on the destriping efficiency. A more comprehensive analysis of the impact of these classes of effects, of their relative weight and of their coupling with the $1/f$ noise will be presented in a future work (Burigana et al. 1999).

As proved by the scientific experience in many years of work in physics, in cosmology and astrophysics, efficient data analysis tools can significantly improve the quality of the information extracted from the data, provided that the systematic effects are well understood, but the first and most important step in projecting experiments is to reduce all the contaminations at the lowest possible levels. It is then of great importance to decrease as much as possible the impact of $1/f$ noise before destriping and $f_{\mathrm{k}} = 0.01$ Hz is an important goal for instrument studies and prototypes.

References

Beccaria M., et al., 1996, "Gravitational wave search: real time data analysis strategies on paralle computers", NTS-96024
Bennet C., et al., 1996a, ApJ 464, L1
Bennet C., et al., 1996b, Amer. Astro. Soc. Meet. 88.05

Bersanelli M., et al., 1995, Int. Rep. TeSRE/CNR 177/1995

Bersanelli M., et al., 1996, ESA, COBRAS/SAMBA Report on the Phase A Study, D/SCI(96)3

Blum E.J., 1959, Ann. Astrophys. 22-2, 140

Burigana C., et al., 1997, Int. Rep. TeSRE/CNR 198/1997, astro-ph/9906360

Burigana C., et al., 1998, A&ASS 130, 551

Burigana C., et al., 1999, A&A (to be submitted)

Colvin R.S, 1961, Ph.D. Thesis, Stanford University

Coolet J.W., Tukey J.W., 1965, "An algorithm for machine calculation of complex Fourier series", Math. Computat. 19, 297

Cuoco E., Curci G., 1997, "Modeling a VIRGO-like noise spectrum - Note 1", VIR-NOT-PIS-1390-095, 14/07/97

Danese L., et al., 1996, Astro. Lett. Comm. 35, 257

De Bernardis P., Masi S., 1998, Proceedings of the XXXIIIrd Rencontres de Moriond, "Fundamental Parameters in Cosmology", Les Arcs, France, January 17-24, 1998, Trân Thanh Vân et al. (eds.), p. 209

Delabrouille J., 1998, A&ASS 127, 555

De Zotti G., et al., 1999, Proceedings of the EC-TMR Conference "3 K Cosmology", Roma, Italy, 5-10 October 1998, AIP Conf. Proc. 476, Maiani L., Melchiorri F., Vittorio N. (eds.), astro-ph/9902103, p. 204

Górski K.M., et al., 1996, ApJ 464, L11

Górski K.M., Hivon E., Wandelt B.D., 1998, to appear in the Proceedings of the MPA/ESO Conference "Evolution of Large Scale Structure", Garching, Germany, August 2-7, 1998, Banday A.J., Sheth R.K., Da Costa L. (eds.), astro-ph/9812350

Heideman M.T., Johnson D.H., Burrus C.S., 1984, "Gauss and the history of the FFT", IEEE Acoustics, Speech and Signal Processing Magazine, Vol. 1, p. 14

Janssen M., et al., 1996, astro-ph/9602009

Kogut A., et al., 1996, ApJ 460, 1

Lasenby A.N., Jones A.W., Dabrowski Y., 1998, Proceedings of the XXXIIIrd Rencontres de Moriond "Fundamental Parameters in Cosmology", Les Arcs, France, January 17-24, 1998, Trân Thanh Vân et al. (eds.), p. 221

Mandolesi N., et al., 1998, Planck LFI, A Proposal (submitted to the ESA)

Puget J.L., et al., 1998, HFI for the Planck Mission, A Proposal (submitted to the ESA)

Schlegel D.J., et al., 1998, ApJ 500, 525

Seiffert M., et al., 1997, Rev. Sci. Instrum. (submitted)

Smoot G.F., et al., 1992, ApJ 396, L1

Strang G., 1976, "Linear Algebra and Its Applications". Academic Press, Inc.

Wandelt B.D., et al., 1999, Communication at the LFI Consortium Meeting, Firenze, 25-26 March 1999

Wandelt B.D., Górski K.M., 1999 (in preparation)

Wright E.L., 1996, in IAS CMB Data Analysis Workshop, Princeton, 22 Nov. 1996, astro-ph/9612006